GFF

ISSN: 1103-5897 (Print) 2000-0863 (Online) Journal homepage: http://www.tandfonline.com/loi/sgff20

Manual extraction of bedrock lineaments from high-resolution LiDAR data: methodological bias and human perception

Thomas Scheiber, Ola Fredin, Giulio Viola, Alexandra Jarna, Deta Gasser & Renata Łapińska-Viola

To cite this article: Thomas Scheiber, Ola Fredin, Giulio Viola, Alexandra Jarna, Deta Gasser & Renata Łapińska-Viola (2015): Manual extraction of bedrock lineaments from high-resolution LiDAR data: methodological bias and human perception, GFF, DOI: 10.1080/11035897.2015.1085434

To link to this article: http://dx.doi.org/10.1080/11035897.2015.1085434

Published online: 16 Nov 2015.

GFF, 2015
http://dx.doi.org/10.1080/11035897.2015.1085434

Article

Manual extraction of bedrock lineaments from high-resolution LiDAR data: methodological bias and human perception

THOMAS SCHEIBER[1], OLA FREDIN[1,2], GIULIO VIOLA[1,3], ALEXANDRA JARNA[1], DETA GASSER[1] AND RENATA ŁAPINSKA-VIOLA[1]

Scheiber, T., Fredin, O., Viola, G., Jarna, A., Gasser, D. & Łapinska-Viola, R., 2015 : Manual extraction of bedrock lineaments from high resolution LiDAR data: methodological bias and human perception. *GFF*, Vol. 00, No. 0, pp. 1–11. © Geologiska Föreningen. doi: http://dx.doi.org/10.1080/11035897.2015.1085434.

Abstract: Manual extraction of topographic features from Light Detection and Ranging (LiDAR) images is a quick, cost effective and powerful tool to produce lineament maps of fractured basement areas. This commonly used technique, however, suffers from several biases. In this contribution, we present the influence of (1) scale, (2) illumination azimuth and (3) operator, which significantly affect results of remote sensing expressed as number, orientation and length of the mapped lineaments. Six operators (N1–N6) with differing experience in remote sensing and different Earth sciences backgrounds mapped the same LiDAR DEM of a fractured bedrock terrain located in western Norway at three different scales (1:20.000, 1:10.000, 1:5.000) and illuminated from three different azimuths (045°, 180°, 315°). The 54 lineament maps show considerable output variability depending on the three factors: (1) at larger scales, both the number and the orientation variability of picked lineaments increase, whereas the line lengths generally decrease. (2) Linear features oriented perpendicular to the source of illumination are preferentially enhanced. (3) Inter-operator result reproducibility is generally poor. Operators have different perceptions of what is a lineament. Ironically, this is particularly obvious for the results of the "most experienced" operators, seemingly reflecting a stronger conceptual bias of what lineaments are and an operational bias on how they should be mapped. Based on these results, we suggest guidelines aimed to improve the reliability of remote sensing lineament interpretations.

Keywords: lineament mapping, fractures, manual interpretation, objective, LiDAR, DEM

[1]Geological Survey of Norway, Trondheim, Norway; thomas.scheiber@ngu.no; [2]Department of Geography, Norwegian University of Science and Technology, Trondheim, Norway; [3]Department of Geology and Mineral Resources Engineering, Norwegian University of Science and Technology, Trondheim, Norway
Manuscript received 13 March 2015; Revised manuscript accepted 04 August 2015.

1. Introduction

Remote sensing technologies provide powerful tools for the identification and analysis of a wide range of geological and geomorphological features (e.g. Smith & Pain 2009). They allow geological mapping in remote areas and over large spatial domains that are difficult or impossible to cover by foot, and permit easier recognition of regional patterns. Remote sensing in Earth sciences has been applied ever since aerial photographs became available and enjoys popularity due to readily available high quality satellite images, together with rapidly improving computing power, and is of great importance particularly in the field of brittle fracture analysis (e.g., Wise et al. 1985; Lowman et al. 1992; Viola et al. 2005; Raharimahefa & Kusky 2009; Oden et al. 2012; Awdal et al. 2013). The high spatial resolution offered by Light Detection and Ranging (LiDAR) datasets, combined with the capability of scanning also through vegetation covers, has revolutionized the production of digital elevation models (DEM). A DEM from LiDAR data commonly shows the Earth's surface in great detail and the ground resolution often approaches or even surpasses 1 m. Relief-shading (hillshade) is the most common method to visualize landforms from DEMs (Smith & Clark 2005), generally with a source of illumination in the northwest. Lineaments perceivable in a DEM are linear features manifested by visual alignments. They can represent any possible discontinuity of planar attitude, including natural geographic features related to bedrock structure or quaternary deposits, as well as animal paths or man-made structures such as roads, railroads, power lines and fences. If they reflect structures in bedrock, they can represent the surface expression of bedding, foliation, faults, fractures or fracture zones and are linked with the local or regional tectonics. Depending on the dip angle of planar structures in bedrock and their interference with the topography, lineaments can be curved in map view.

There are essentially two approaches to extract lineament information from images: (a) automated quantitative analysis by using remote sensing/GIS software and (b) manual interpretation by a human operator. Manual interpretation

is well suited for spatial assessment but poor in quantitative accuracy (e.g., Richards & Jia 2006). On the other hand, automatically generated lineament maps have been found to contain a higher lineament density and a more uniform distribution of orientations than manually produced lineament maps (Vaz et al. 2012).

The availability of software tools and guidelines to analyze image data, for example to (semi-) automatically detect lineaments, has strongly increased in the past decade (e.g., Raghavan et al. 1995; Wladis 1999; Gloaguen et al. 2007; Rutzinger et al. 2007; Masoud & Koike 2011; Soto-Pinto et al. 2013). Nevertheless, visual manual interpretation, commonly carried out by one person only, remains a common technique to produce lineament maps (e.g., Gabrielsen et al. 2002; Ustaszewski & Pfiffner 2008; Jacques et al. 2012; Viola et al. 2012; Domínguez-González et al. 2015).

This notwithstanding, since the beginning of manual lineament mapping on aerial photographs, it has been shown that the mapping results can differ largely between different operators, questioning the reproducibility of manual lineament extraction (e.g., Burns et al. 1967; Podwysocki et al. 1975; Burns & Brown 1978; Huntington & Raiche 1978). Differences between operators are also obvious in a recent mapping study using a synthetic DEM of a drumlin field (Hillier et al. 2014). Also, in addition to the influence of operator variability and human perception, technical factors such as (1) the relation between the feature size to the spatial resolution, (2) the angle between the feature orientation and illumination direction, and (3) the tonal and textural information in the image have been shown to influence the results of remote sensing analyses (e.g., Smith & Wise 2007).

Despite previous studies indicating that several factors do indeed influence the reliability of the still widely used eye-based lineament analysis, suggestions on how to standardize interpretation methods are still lacking. In an attempt to develop such a standardization, we present a lineament mapping case study using a LiDAR DEM of a fractured bedrock region in SW Norway. We investigated three factors with potential significance for the interpretation: (1) scale, (2) illumination azimuth and (3) operator. We elaborate here on the influence of each of these factors on several output parameters such as number, orientation and length of lineaments. We present a unique dataset that shows considerable output variability depending on the three chosen factors, which in turn questions the reliability of manually produced one-operator lineament maps. Based on these results, we suggest an operational workflow for the extraction of lineaments from LiDAR datasets, which, if followed, can contribute to significantly improved reliability of the data extracted from manual analysis.

2. Lineament patterns in the study area

The Rolvsnes granodiorite (Andersen & Jansen 1987; Andersen et al. 1991), exposed on the Bømlo islands in SW Norway (Fig. 1a), is a late-Caledonian intrusive body that escaped penetrative ductile strain but was affected by multiple brittle deformation episodes since the time of its emplacement (Ksienzyk 2011). Recently obtained LiDAR data provide a high-resolution view of the ground, which in turn can be used to extract bedrock lineament patterns. The islands are covered by only sparse vegetation and minimal quaternary deposits so that the LiDAR data closely reflects the bedrock surface. In the analyzed area, bedrock lineaments can be regarded as surface manifestation of generally steeply dipping fault- and fracture zones. The bedrock lineament trends are closely linked to the post-Caledonian brittle deformation history of SW Norway, which accommodated at least two main episodes of extension (e.g., Larsen et al. 2003). NE–SW striking lineaments represent mainly dip-slip faults resulting from NW–SE extension, whereas N–S to NNW–SSE striking lineaments can be mostly attributed to an episode of E–W extension. This is generally associated with alkaline dyke intrusions concentrated along NNW–SSE striking lineaments in the Sunnhordland area (Valle et al. 2002). The nature of NW–SE striking lineaments is not entirely clear, but a multiphase reactivation history has been suggested (op. cit.).

3. Experimental setup

A 5 × 5 km^2 area within the Rolvsnes granodiorite covering the island of Goddo (Fig. 1b) was chosen as target area for our study. The LiDAR data used in the experiment was scanned from aircraft in 2012 with a point cloud density varying between 0.38 and 3.40 points/m^2. Average point spacing is approximately 1.2 points/m^2. The point cloud was gridded, using "last returns" only to exclude vegetation and infrastructure, to a DEM with resolution of 1 m using standard binning interpolation in ArcGIS. The DEM appears to be of very high quality with few artifacts, and field check confirms that the DEM represents actual topography very well. Three hillshaded images illuminated from three different azimuths were generated using an inclination of 045° (Table 1; Fig. 1c–e). Illumination azimuths were chosen at 045°, 180° and 315°, 315° being the most commonly used orientation. These differently illuminated images were mapped at the scales of 1:20.000, 1:10.000 and 1:5.000, resulting in a total of nine mapping exercises for each person. Assuming a computer screen resolution of 96 dpi and a DEM resolution of 1 m, these mapping scales correspond to objects on the ground with sizes of 5.3, 2.6 and 1.3 m, respectively. In other words, at the 1:20.000 scale linear objects thinner than 5.3 m will hardly be seen. At the 1:5.000 mapping scale the smallest observable features are about 1 m wide and close to the resolution of the hillshaded DEM. The sequence of mapping of the nine different exercises was set such that both scale and illumination direction were changed between every single experiment (Table 1) in order to minimize the bias that would be otherwise induced by successive picking exercises carried out under identical boundary conditions.

Six persons currently employed at NGU (Geological Survey of Norway) with different backgrounds in Earth sciences and different experiences in remote sensing techniques were selected for the study. Operators N1, N3 and N4 have previous experiences in manual lineament mapping whereas N2, N5 and N6 have none. N1, N4 and N5 have a background in geomorphology and N2, N3 and N6 have a background in bedrock mapping and structural geology. Each received an ArcGIS file geodatabase together with detailed practical instructions on how to carry out the mapping exercises. Operators were requested to aim at mapping fracture lineaments in the whole image by drawing straight lines only. A scale-dependent time limit was set at 8 min for the 1:20.000 scale, 30 min for the 1:10.000 scale and 120 min for the 1:5.000

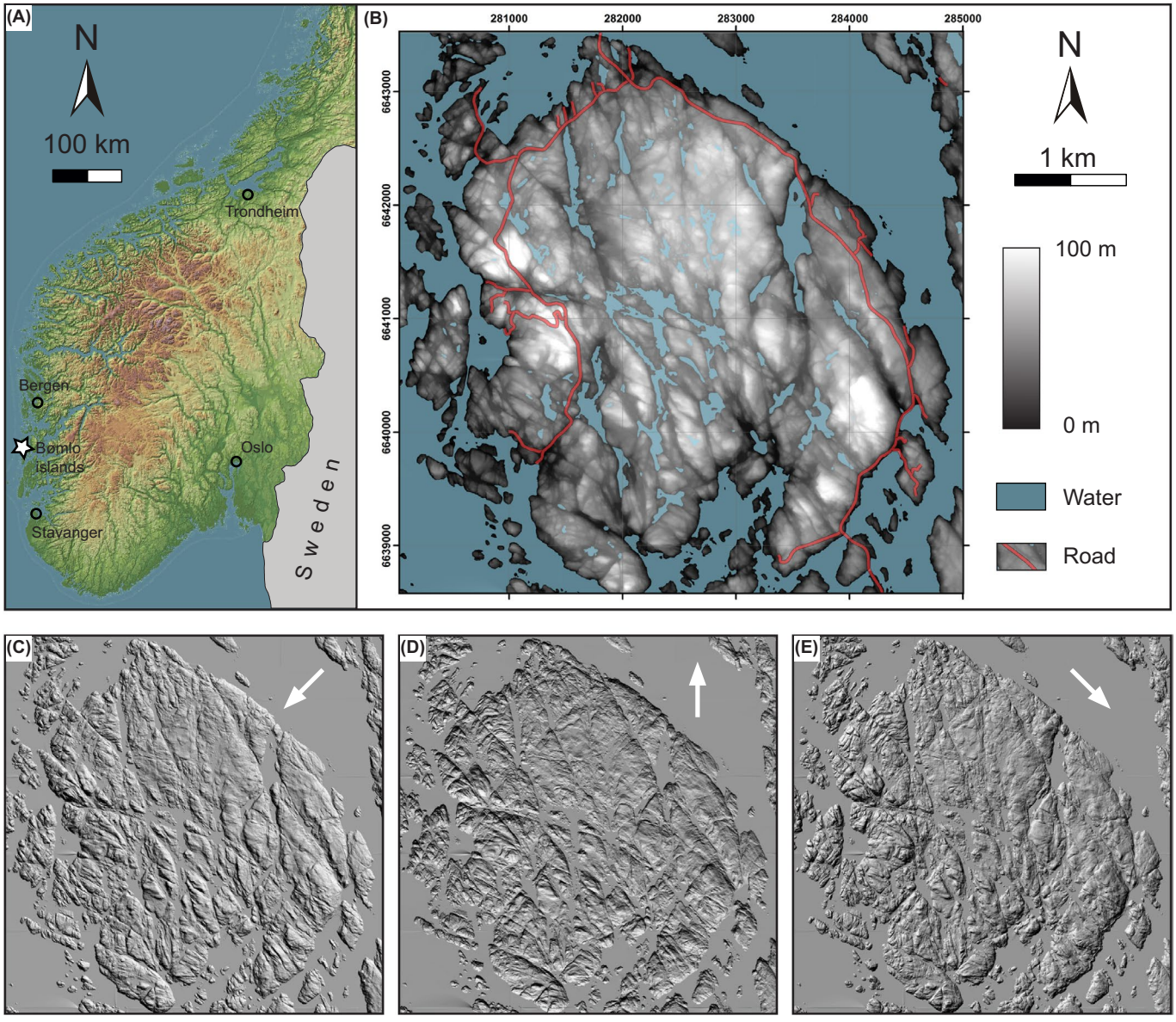

Fig. 1. (**A**) Relief map of mid- and southern Norway. Star indicates the location of the study area. (**B**) LiDAR DEM of the Goddo island. (**C**–**E**) Hillshaded DEMs highlighting fracture patterns on Goddo island. Different illumination azimuth angles are indicated by white arrows. Solar elevation is 045° for all hillshade images.

Table 1. Numbers 1–9 indicate the order of the different mapping exercises.

		Scale		
		1:20.000	1:10.000	1:5.000
Illumination azimuth	045°	1	8	6
	315°	4	2	9
	180°	7	5	3

scale. It was not allowed to change the scale during one mapping exercise. Turning on and off layers showing roads and lakes was allowed. Computer screen and screen resolution settings were identical for all persons.

The six operators extracted lineaments from the same area at three different scales and illuminated from three different directions, totaling 54 datasets. Each person mapped what he or she considered to be bedrock fractures.

4. Data analysis and visualization

Examples of some of the produced lineament maps are presented in Fig. 2. Rose diagrams with a linear radial scale for frequency are commonly used to plot data in the polar domain, and are known for their sensitivity to the choice of bin width and starting point (Wells 1999; Davis 2002). Therefore, we present the data of each mapping experiment by means of equal-area

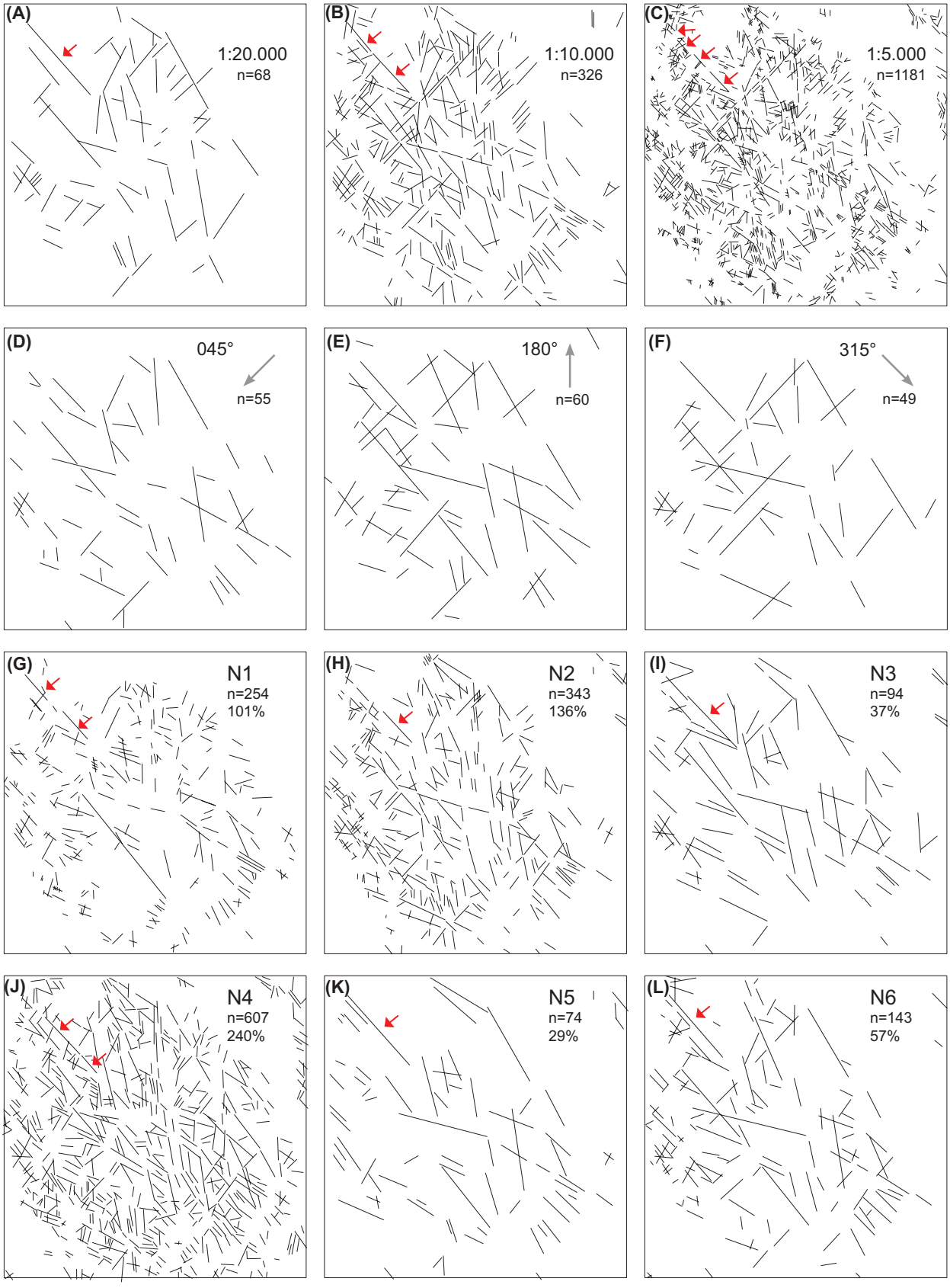

Fig. 2. Examples of lineament maps showing the contrasting results arising from the different investigated factors. (**A**–**C**) Influence of scale exemplified by lineament maps obtained by N2 at 315° illumination azimuth. Red arrows point to the same linear feature which was drawn as one lineament at the 1:20.000 scale, but was interpreted to consist of multiple segments at larger scales. (**D**–**F**) Influence of illumination azimuth shown for lineament maps produced by N6 at the 1:20.000 scale. Gray arrows indicate illumination azimuth. (**G**–**L**) Influence of operator variability presented for the exercise performed at the 1:10.000 scale and illuminated from 045°. Number of lineaments is given as total number (***n***) and as percentage to the average number of lines drawn during this exercise. Red arrows indicate the same feature as pointed out in (**A**–**C**), which was recognized by all operators, but was drawn as one line by some operators (although with different lengths) and interpreted to consist of two segments by others.

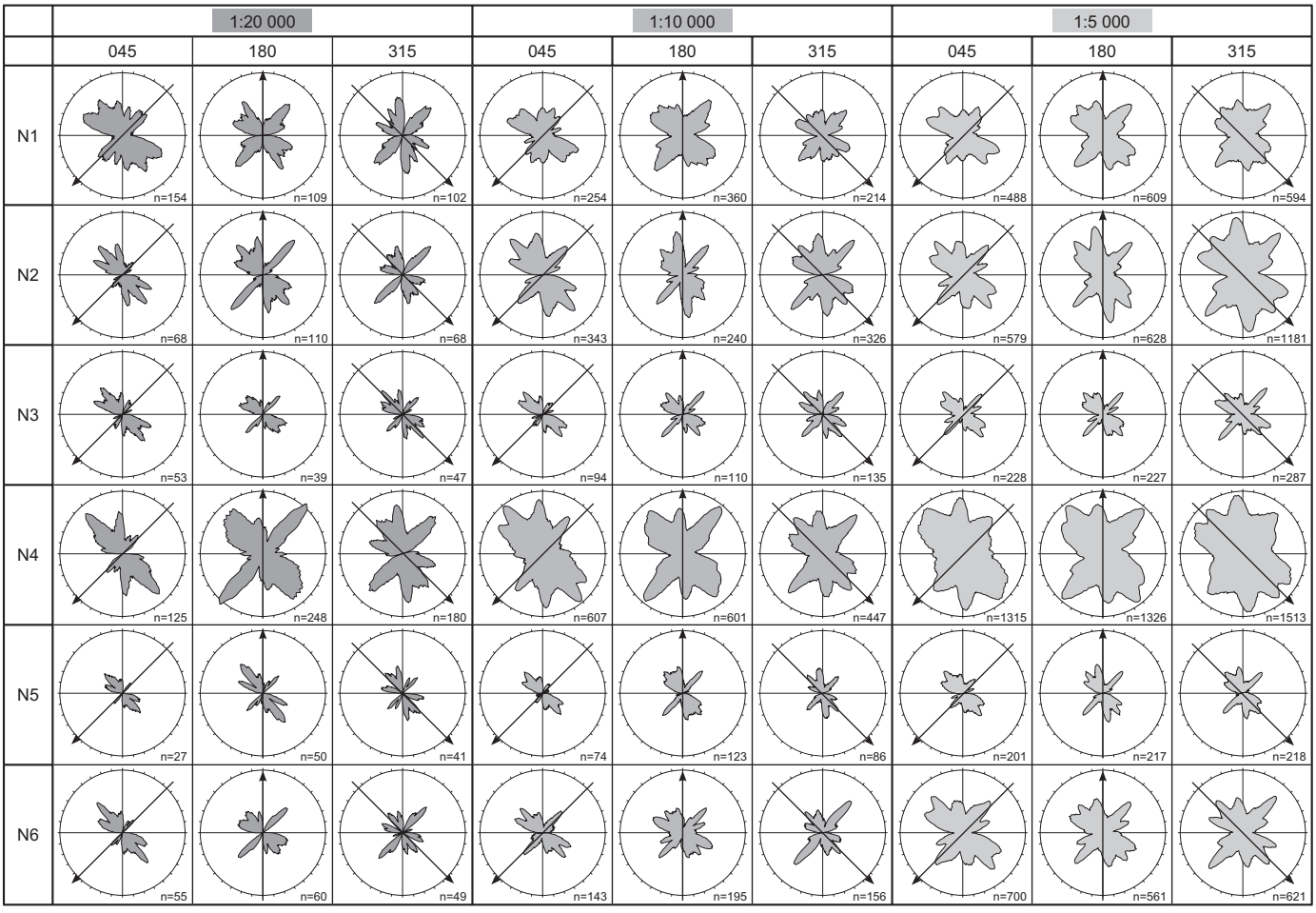

Fig. 3. Moving average rose diagrams and corresponding number of lineaments for each mapping exercise. Arrows indicate the illumination azimuth, gray shades indicate scale. Outer circle of rose diagrams corresponds to a weighted moving average value of 2 for 1:20.000 scale plots, 3 for 1:10.000 scale plots and 4 for 1:5.000 scale plots. Aperture = 13°, weighting factor = 0, 9 for all plots.

moving average rose diagrams (Fig. 3) produced by the MARD application of Munro and Blenkinsop (2012). This software filters the data such that angular datasets are smoothened, significant circular trends are emphasized and background noise is reduced. In addition, the mapping results are synthesized in the form of normalized probability density plots (Fig. 4) and cumulative distribution functions (Fig. 5), which facilitate a critical comparison of the different datasets. In Figs. 4 and 5, each curve represents the sum of orientation data from several mapping exercises. In Figs. 4 and 5a–c, each curve sums up the three datasets (illuminated from 045°, 180° and 315°) obtained by one operator at a specific scale and is thus representative for the mapping of each individual operator. In Fig. 5d–f, the mapping results obtained by all operators at a specific scale and illumination are summarized in a data series. Merging datasets minimizes the influence of outliers, and at the same time, improves the critical comparison of the individual data series.

5. Results

5.1. *Number of mapped lineaments*

The number of mapped lineaments varies between 27 and 248 at the 1:20.000 scale, between 74 and 607 at 1:10.000 and between 201 and 1513 at 1:5.000 scale as a function of the three factors investigated (Fig. 3). Operator N5 invariably mapped the least number of lineaments, whereas N4 mapped the most. There is a general increase in the number of mapped lineaments toward larger scales (Fig. 3) since the operators obviously detect more lineaments at 1:5.000 compared to 1:10.000 or 1:20.000 (Fig. 2a–c). The number of mapped lineaments also varies with the different illuminations within one scale, but no obvious systematics could be recognized.

5.2. *Orientation of mapped lineaments*

Each of the three considered factors exerts considerable influence on the recorded orientation of the mapped lineaments.

(1) Influence of scale: The positions of the normalized orientation frequency maxima obtained by the operators change with the scale (Fig. 4), but no systematic correlation between scale and orientation maxima could be observed. For the mapping exercises carried out by operator N5 and also for the total dataset (“All data” in Fig. 4), the two first orientation maxima overlap at all scales. The heights of the maxima, however, are

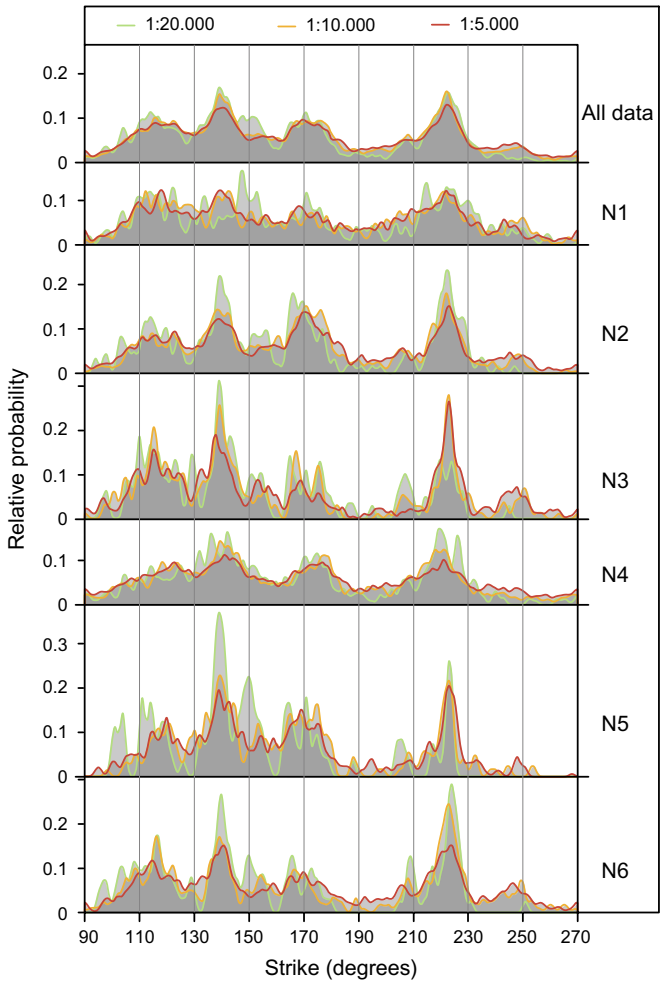

Fig. 4. Normalized probability density plots including all the lineaments mapped by individual operators at a specific scale. "All data" includes the results obtained by all operators at a specific scale.

scale-dependent and peaks are generally more subdued at larger scales (Fig. 4). This indicates that the variability in mapped orientations becomes higher at larger scales, which, in turn, explains why rose diagrams generally have less distinct spatial trends (Fig. 3) and slope changes in the cumulative distribution functions are less pronounced at larger scales (Fig. 5). Furthermore, the larger the scale, the more similar are the orientation results of the six operators (Fig. 5a–c) and the more similar are also the results obtained from the differently illuminated images (Fig. 5d–f).

(2) Influence of illumination azimuth: There are significant differences between the mapping exercises performed on DEMs illuminated from 045° and those illuminated from 315°. These differences can be best appreciated at the 1:20.000 scale (Figs. 2d, e and 5d). Lineaments oriented perpendicular to the illumination direction are detected more easily than lineaments with other orientations. The results from the DEM illuminated from 180° are significantly different from the other two data series and broadly represent an intermediate result. Lineaments plotting within the first and third quadrant of the rose diagram, however, show a striking similarity to the 315° data series. The larger the scale, the more similar the data series become and the less drastic the differences between different illuminations. Data series 180° and 315° can be regarded as similar at the 1.10.000 and 1:5.000 scales (Fig. 5e, f).

(3) Influence of operator: All mapping exercises generally exhibit a large number of c. NW–SE and NE–SW striking lineaments, and a low frequency of c. E–W striking lineaments (Figs. 3–5). Two additional minor lineament trends strike WNW–ESE and NNW–SSE, respectively. When looking in detail at the mapping results obtained (Figs. 2 and 3), however, some considerable differences can be recognized. Several rose diagrams have significantly different shapes, even if the number of mapped lineaments is approximately the same (e.g., N1 vs. N4 at 1:20.000 and 045°, N2 vs. N6 at 1:10.000 and 180°, N3 vs. N5 at 1:5.000 and 315°; Fig. 3).

The most remarkable discrepancies in the compiled orientation patterns can be recognized between operators N1 and

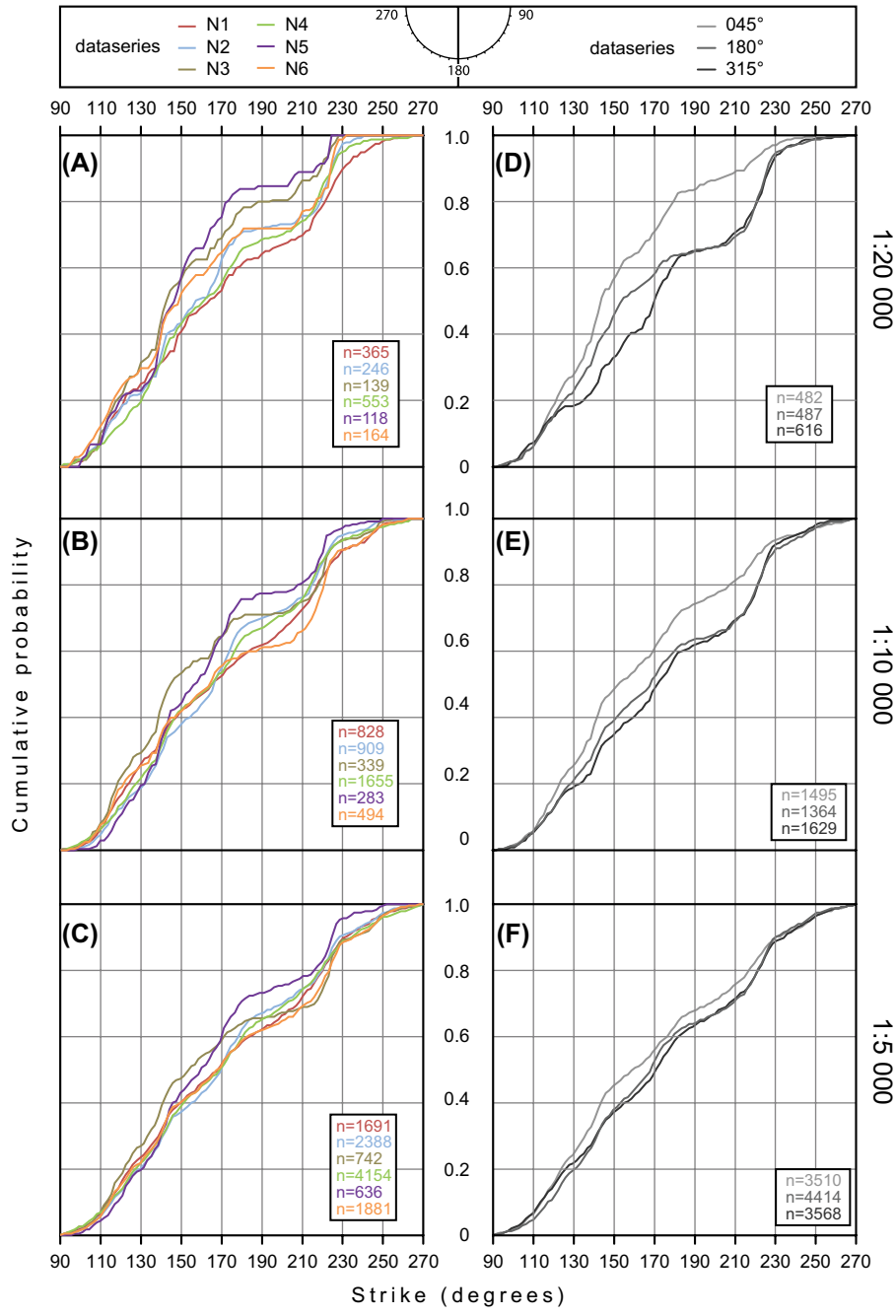

Fig. 5. Cumulative distribution functions for the sum of all lineaments drawn by the individual operators at the (**A**) 1:20.000 scale, (**B**) 1:10.000 scale and (**C**) 1:5.000 scale. Cumulative distribution functions for the sum of all lineaments drawn by all operators at a specific illumination azimuth at the (**D**) 1:20.000 scale, (**E**) 1:10.000 scale and (**F**) 1:5.000 scale. Note that plots start at a strike of 90°.

N5 at the 1:20.000 scale (Fig. 5a) and between N5 and N6 at the 1:10.000 scale (Fig. 5b). At the 1:5.000 scale, the differences become less pronounced, but N5 still shows the most peculiar orientation pattern, with the most pronounced slopes in the cumulative distribution function, indicating a low variability in orientations (Fig. 5c). This reflects the fact that operator N5 has mapped the lowest numbers of lineaments. The datasets of N1 and N4 show the smallest peaks on the normalized probability density plots (Fig. 4) and therewith exhibit a high variability in lineament orientations at all scales (Figs. 4 and 5).

Another interesting mapping behavior can be seen when considering the apparent correlation between the output parameters orientation and the number of drawn lineaments: the number of drawn lines has an apparent influence on the general shape of the moving average rose diagram, irrespective of the scale, wherein the more abundant the lines, the less accentuated the shape of the rose diagram (Fig. 3). This indicates that operators who detected a large number of lineaments are likely to trace more features that are misoriented to the major and rather obvious regional trends than operators who pick fewer lines.

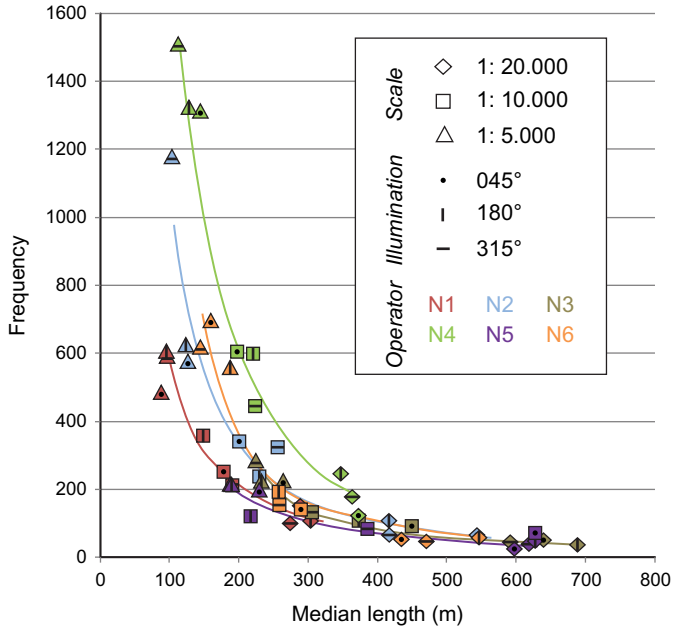

Fig. 6. Median lineament length versus frequency diagram for all data-sets. Power trend lines for each operator indicate the scale dependency.

5.3. *Length of the mapped lineaments*

Output parameters length and number of drawn lineaments are interestingly correlated, whereby the higher the number of lineaments, the shorter the line lengths median (Fig. 6). As in the case of the number and orientation of detected lineaments, the length is dependent on the three factors scale, illumination azimuth and operator.

(1) Influence of scale: The lengths of the drawn lines are strongly dependent on the scale: as to be expected, the larger the scale, the shorter the lines (Figs. 2a–c and 6a). Similarly, the standard deviations of line lengths decrease with larger scales (Fig. 7).

(2) Influence of illumination azimuth: Mapped line lengths also vary somewhat with the different illumination directions (for example N5 at 1:10.000), but no systematic relationship can be seen (i.e. the longest lineaments are not always drawn at the same illumination, Fig. 6a).

(3) Influence of operator: The line lengths vary considerably depending on the operator. The medians of the line lengths of N1, for example, are consistently the lowest at all scales, whereas N3 and N5 drew the longest lines at all scales, and N4 always drew shorter lines than N6 at all scales (Fig. 6, cf. Fig. 2g, h). An interesting aspect concerning line lengths is shown in Fig. 7. The calculated linear trend lines indicate how the length of the picked lineaments changed (if at all) as each mapping session progressed and thus provide insights into the mapping behavior of the operators. A steep line means that the operator started their assignment by picking long lineaments and drew progressively shorter lines toward the end, whereas a flat line indicates that the mapper drew lineaments with similar lengths throughout the exercise. Steep lines are prevalent in the 1:20.000 exercises, whereas rather flat lines generally characterize the 1:5.000 exercises. N1 drew lines of similar lengths throughout each individual exercise, whereas N3 shows a clear tendency of drawing progressively shorter lines as the assignment progressed. In some of the exercises, however, the lines have positive slopes, which points to the opposite relation. The slope of these lines is apparently correlated with the calculated standard deviations of line lengths (Fig. 7). The generally flat lines for N1 and N4 are associated with low standard deviation values, whereas the steep lines for N3 and N5 have the highest standard deviation values.

6. Summary and discussion

6.1. *Scale variance*

The choice of mapping scale has a clear influence on the number, orientation and length of mapped lineaments. The larger the scale, the more lineaments are drawn. The variability in orientation data increases with larger scales, which can be recognized by the less distinct spatial trends of the rose diagrams (Fig. 3) and by the approximately straight cumulative distribution functions (Fig. 5) for the 1:5.000 mapping results. At the same time, the differences in median line lengths become less pronounced with larger scales (Fig. 6) and standard deviation values of line lengths decrease (Fig. 7). Features that are interpreted as one lineament at the 1:20.000 scale are interpreted as a collection of multiple smaller lineaments at larger scales (Fig. 2a–c). This is due to the ability to recognize greater details at larger scales. Therefore, manually produced lineament maps have to be regarded as scale-variant and thus display a non-fractal behavior (Barton 1995; Gloaguen et al. 2007). Mapping at multiple scales is therefore

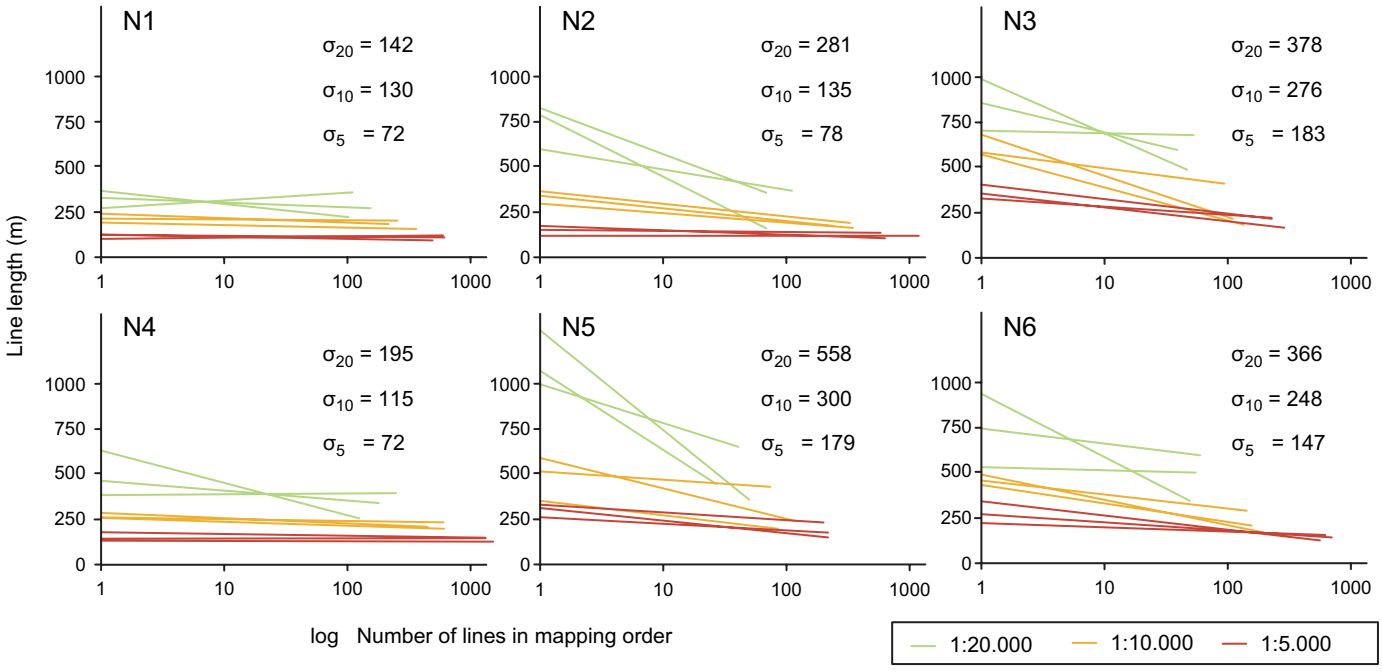

Fig. 7. Linear trend lines highlighting the line lengths mapping history for each exercise. Lines of the same color derive from mapping exercises at the same scale, but different illuminations. Standard deviations of line lengths (meters) are provided for the mapping exercises performed at the 1:20.000 (σ_{20}), 1:10.000 (σ_{10}) and the 1:5.000 scale (σ_5).

of great importance because it can help to highlight the potential role of fundamental geological processes that control lineament distribution and characteristics as a function of scale.

6.2. *Illumination bias*

Linear features oriented perpendicular to or at a high angle to a given illumination azimuth are preferentially enhanced. Lineament mapping of a DEM illuminated from only one azimuth direction can therefore lead to a strong bias potentially resulting in the complete overlooking of some significant lineament trends. To eliminate the bias introduced by single azimuth illumination, it has been suggested to use at least two illumination angles, perpendicular and parallel to the dominant fracture trend (e.g., Graham & Grant 1991; Smith & Clark 2005). This has been done in the present study, and, indeed, the DEMs illuminated from 045° to 315° resulted in different orientation patterns enhancing lineaments perpendicular to the illumination azimuth, most pronounced at the 1:20.000 scale (Figs. 2d, e and 5). In addition, we have also used an illumination azimuth of 180°, which gives similar lineament patterns as the ones generated on DEMs illuminated from 315°, especially at the 1:10.000 and 1:5.000 scales (Fig. 5e, f). Differences between the 315° and 180° illumination azimuths are restricted to the frequency of c. NW–SE (125–180°) striking lineaments, which can be best seen in the 1:20.000 mapping exercise (Fig. 5d). The reason why the 180° illumination is similar to the 315° and not the 045° illumination might be a truly higher density of c. NE–SW striking lineaments in the study area. It might also reflect, however, a real difference in the characteristics of the two trends in terms of dip azimuth and dip angle of the fracture planes, length and density of lineaments and/or incision depth. These factors exert a true influence on the landform expression in the image (Smith & Wise 2007), resulting in preferential enhancing of the NE–SW striking lineaments. This makes it obvious that the ideal choice of number and orientation of azimuth illuminations in lineament mapping is dependent on the real fracture pattern in the study area and should be evaluated from case to case. Preliminary fracture pattern extraction from the original (un-shaded) DEM, or non-directional image enhancement, such as slope, are valid possibilities to evaluate the ideal illumination configurations for each study.

Another factor which potentially influences the results of lineament mapping, but which has not been tested in our experiments, is the choice of the solar inclination angle, which in essence affects the length and deepness of shadows and can enhance relief. High contrast images are obtained by low solar inclination angles and enable detection of smooth landforms, as found in glacial terrains (e.g., Aber et al. 1993; Jansson & Glasser 2005). However, for shaded relief interpretations of bedrock fracture patterns, where variations in slope occur on small horizontal distances, a 045° inclination angle is commonly suggested (e.g., Masoud & Koike 2006; Jacques et al. 2012) and was thus used in our experiments.

6.3. *Operator variability*

Our study shows that there exist considerable differences among the individual operators with respect to the number, orientations and lengths of the digitized lineaments (Figs. 2g-l, 3, 4, 5 and 6), and that the decision of "which lineament represents a structural feature" is subjective. Personal styles and preferences of the interpreters are evident in the different mapping exercises. Some operators chose to draw a large number of lineaments, resulting in a great variability of orientations (N1, N4), whereas others were more conservative by drawing fewer lineaments with a

smaller variability of orientations (N3, N5). Features that are interpreted as one lineament by some operators were interpreted as a collection of multiple smaller lineaments by other operators (Fig. 2g–l). The effect of operator variability on the lineament orientations is the greatest at the small scales, i.e. 1:20.000. The variability of line lengths of the drawn lineaments is low for N1 and N4 and high for N3 and N5 (standard deviation values in Fig. 7). Some mappers drew lineaments of similar length during the entire mapping exercise (N1, N2 and N4 at the 1:5.000 scale), whereas others drew first long and then shorter lines (N3, N5, N6). However, some results also show the opposite relationship (Fig. 7). This implies that the lengths of lineaments mapped is not necessarily a result of the number of lineaments, but also a function of the mapper's decision on what feature they interpret as a meaningful lineament and what they discard as not geologically true.

No correlations can be seen with respect to experience or professional background of the operators. N2 and N4 show the highest agreement in orientation patterns (Fig. 5a–c), but have neither the same professional background nor similar experience in lineament mapping. The lineament maps of the "most experienced" operators N1, N3 and N4 represent extreme mapping results. N1 drew constantly the shortest lines, which at the same time have the highest variability in azimuth values in all mapping exercises. Consequently, the mapping performed by this operator resulted in rose diagrams having the least defined orientation trends (Figs. 3 and 4). The results obtained by N3 are characterized by very low numbers of lineaments and, as a result, rose diagrams exhibit distinct spatial trends. In contrast, the mapping results of N4 comprise by far the highest number of lineaments. These results show that manually produced lineament maps are strongly influenced by personal mapping style, and that the reproducibility among different operators is poor, which is especially the case for the "most experienced" operators.

7. Conclusions

Mapping of linear features using a high-quality LiDAR-derived hillshade model is generally perceived as straightforward and can be accomplished regardless of experience and training. However, the present study highlights several pit-falls with this approach. There is a strong dependence of manually produced lineament maps on at least scale, illumination azimuth and operator, the three factors of bias investigated in our study. The number, orientation and length of the mapped lineaments vary considerably from exercise to exercise, and the reproducibility of the output is in general poor. Therefore, caution should be applied when relying on man-made lineament maps produced by a single operator.

In order to minimize the bias and increase reproducibility in future studies, we propose the following guidelines:

(a) In every lineament mapping study, it is important to define clearly from the beginning the mapping goals. The choice of mapping scale depends on the goal of the project and has to be evaluated case by case.

(b) Our study shows that mapping at smaller scales (e.g., 1:20.000) results in more pronounced orientation trends and thus might represent regional geological trends better than mapping at larger scales (e.g., 1:5.000). However, reproducibility between operators is poorer at smaller scales. It should be noted that operator time expenditure quadruples each time the scale is doubled, so that mapping at 1:5.000 takes roughly eight times longer than mapping at 1:20.000. Thus, care should be taken to find a mapping scale that is appropriate to the goals of the study as defined in (a). The high resolution of LiDAR data allows for very detailed mapping, which is not always warranted by the mapping project.

(c) In order to establish the ideal illumination azimuths, it is recommended to test at least two complementary orientations that are perpendicular or at high-angle to the most obvious lineament sets. Care must be taken so that important trends are not underrepresented due to an unfortunate choice of illumination direction. This evaluation should be done using for example a slope map that is independent of illumination directions.

(d) In a remote sensing project with several persons included, it is important to agree on a given common view on the data, i.e. operators should agree on definitions, mapping scale and tolerance. This can be done by the preliminary mapping of a small test area by each participant followed by the critical analysis of the obtained results so as to highlight obvious issues that may have emerged. Different types of mapping behavior, such as the length of segments and the number of mapped landforms per unit area, should also be discussed. This approach will lead to the harmonization of views and opinions and will increase reproducibility among operators and facilitate the merging of adjacent datasets obtained by different operators.

(e) Operators should always be aware of the human perception bias, and think critically of their own shortcomings when mapping. Readers of papers and maps where only one or very few operators have mapped an area for lineaments, should be aware of the biases discussed in this paper and should question the robustness of the data.

(f) Any remote sensing study has to be regarded as a preliminary exercise and, ideally, should be followed by fieldwork and ground truthing of the obtained results.

Acknowledgments This study was conducted as part of the BASE project, a joint industry project funded by Det Norske, Lundin, Mærsk, Wintershall and the Geological Survey of Norway. Karl Fabian is thanked for stimulating discussions. Pietari Skyttä and an anonymous reviewer are acknowledged for constructive reviews.

Disclosure statement

No potential conflict of interest was reported by the authors.

References

Aber, J.S., Spellman, E.E. & Webster, M.P., 1993: Landsat remote sensing of glacial terrain. *In* J.S. Aber (ed.): *Glaciotectonics and Mapping Glacial Deposits. Proceedings of the INQUA Commission on Formation and Properties of Glacial Deposits*, 215–225. University of Regina, Regina.

Andersen, T.B. & Jansen, Ø.J., 1987: The Sunnhordland Batholith, W. Norway: regional setting and internal structure, with emphasis on the granitoid plutons. *Norsk Geologisk Tidsskrift 67*, 159–183.

Andersen, T.B., Nielsen, P., Rykkelid, E. & Sølna, H., 1991: Melt-enhanced deformation during emplacement of gabbro and granodiorite in the Sunnhordland Batholith, west Norway. *Geological Magazine 128*, 207–226.

Awdal, A.H., Braathen, A., Wennberg, O.P. & Sherwani, G.H., 2013: The characteristics of fracture networks in the Shiranish Formation of the Bina Bawi Anticline; comparison with the Taq Taq Field, Zagros, Kurdistan, NE Iraq. *Petroleum Geoscience 19*, 139–155.

Barton, C.C., 1995: Fractal analysis of scaling and spatial clustering of fractures. *In* C.C. Barton & P.R. La Pointe (eds.): *Fractals in the Earth Sciences*, 141–178. Springer, Berlin.

Burns, K.L. & Brown, G.H., 1978: The human perception of geological lineaments and other discrete features in remote sensing imagery: signal strengths, noise levels and quality. *Remote Sensing of Environment 7*, 163–176.

Burns, K.L., Shepherd, J. & Berman, M., 1967: Reproducibility of geological lineaments and other discrete features interpreted from imagery: measurement by a coefficient of association. *Remote Sensing of Environment 5*, 267–301.

Davis, J.C., 2002: *Statistics and data analysis in geology*, 3rd ed. John Wiley & Sons, New York, NY. 656 pp.

Domínguez-González, L., Andreani, L., Stanek, K.P. & Gloaguen, R., 2015: Geomorpho-tectonic evolution of the Jamaican restraining bend. *Geomorphology 228*, 320–334.

Gabrielsen, R.H., Braathen, A., Dehls, J. & Roberts, D., 2002: Tectonic lineaments of Norway. *Norwegian Journal of Geology 82*, 153–174.

Gloaguen, R., Marpu, P.R. & Niemeyer, I., 2007: Automatic extraction of faults and fractal analysis from remote sensing data. *Nonlinear Processes in Geophysics 14*, 131–138.

Graham, D.F. & Grant, D.R., 1991: A test of airborne, side-looking synthetic-aperture radar in central Newfoundland for geological reconnaissance. *Canadian Journal of Earth Sciences 28*, 257–265.

Hillier, J.K., Smith, M.J., Armugam, R., Barr, I., Boston, C.M., Clark, C.D., Ely, J., Fankl, A., Greenwood, S.L., Gosselin, L., Hättestrand, C., Hogan, K., Hughes, A.L.C., Livingstone, S.J., Lovell, H., McHenry, M., Munoz, Y., Pellicer, X.M., Pellitero, R., Robb, C., Roberson, S., Ruther, D., Spagnolo, M., Standell, M., Stokes, C.R., Storrar, R., Tate, N.J. & Wooldridge, K., 2014: Manual mapping of drumlins in synthetic landscapes to assess operator effectiveness. *Journal of Maps 11*, 719–729.

Huntington, J.F. & Raiche, A.P., 1978: A multi-attribute method for comparing geological lineament interpretations. *Remote Sensing of Environment 7*, 145–161.

Jacques, P.D., Machado, R. & Nummer, A.R., 2012: A comparison for a multiscale study of structural lineaments in southern Brazil: LANDSAT-7 ETM+ and shaded relief images from SRTM3-DEM. *Anais da Academia Brasileira de Ciências 84*, 931–942.

Jansson, K.N. & Glasser, N.F., 2005: Using Landsat 7 ETM+ imagery and Digital Terrain Models for mapping glacial lineaments on former ice sheet beds. *International Journal of Remote Sensing 26*, 3931–3941.

Ksienzyk, A. K., 2011: *From mountains to basins: geochronological case studies from southwestern Norway, Western Australia and East Antarctica*. PhD dissertation. University of Bergen, Bergen. 162 pp.

Larsen, Ø., Fossen, H., Langeland, K. & Pedersen, R.-B., 2003: Kinematics and timing of polyphase post-Caledonian deformation in the Bergen area, SW Norway. *Norwegian Journal of Geology 83*, 149–165.

Lowman, P.D., Jr, Whiting, P.J., Short, N.M., Lohmann, A.M. & Lee, G., 1992: Fracture patterns on the canadian shield: a lineament study with landsat and orbital radar imagery. *In* R. Mason (ed.): *Basement Tectonics 7*, vol. 1, 139–159. Proceedings of the International Conferences on Basement Tectonics. Springer, Berlin.

Masoud, A. & Koike, K., 2006: Tectonic architecture through Landsat-7 ETM+/SRTM DEM-derived lineaments and relationship to the hydrogeologic setting in Siwa region, NW Egypt. *Journal of African Earth Sciences 45*, 467–477.

Masoud, A.A. & Koike, K., 2011: Auto-detection and integration of tectonically significant lineaments from SRTM DEM and remotely-sensed geophysical data. *ISPRS Journal of Photogrammetry and Remote Sensing 66*, 818–832.

Munro, M.A. & Blenkinsop, T.G., 2012: MARD – A moving average rose diagram application for the geosciences. *Computers & Geosciences 49*, 112–120.

Oden, M.I., Okpamu, T.A. & Amah, E.A., 2012: Comparative analysis of fracture lineaments in Oban and Obudu areas, SE Nigeria. *Journal of Geography and Geology 4*, 36–47.

Podwysocki, M. H., Moik, J. G. & Shoup, W. C., 1975: Quantification of geologic lineaments by manual and machine processing techniques. Proceedings of the NASA Earth Resources Survey Symposium TMS-58168 v1B, 885–905.

Raghavan, V., Masumoto, S., Koike, K. & Nagano, S., 1995: Automatic lineament extraction from digital images using a segment tracing and rotation transformation approach. *Computers & Geosciences 21*, 555–591.

Raharimahefa, T. & Kusky, T.M., 2009: Structural and remote sensing analysis of the Betsimisaraka Suture in northeastern Madagascar. *Gondwana Research 15*, 14–27.

Richards, J.A. & Jia, X., 2006: *Remote sensing digital image analysis*. Springer, Berlin. 364 pp.

Rutzinger, M., Maukisch, M., Petrini-Monteferri, F. & Stötter, J., 2007: Development of algorithms for the extraction of linear patterns (lineaments) from airborne laser scanning data. *In* A. Kellerer-Pirklbauer, M. Keiler, C. Embleton-Hamann & J. Stötter (eds.): *Geomorphology for the future: Obergurgl, Austria, Setember 2–7, 2007; Conference Proceedings*, 161–168. Innsbruck University Press, Innsbruck.

Smith, M.J. & Clark, C.D., 2005: Methods for the visualization of digital elevation models for landform mapping. *Earth Surface Processes and Landforms 30*, 885–900.

Smith, M.J. & Pain, C.F., 2009: Applications of remote sensing in geomorphology. *Progress in Physical Geography 33*, 568–582.

Smith, M.J. & Wise, S.M. 2007: Problems of bias in mapping linear landforms from satellite imagery. *International Journal of Applied Earth Observation and Geoinformation 9*, 65–78.

Soto-Pinto, C., Arellano-Baeza, A. & Sánchez, G., 2013: A new code for automatic detection and analysis of the lineament patterns for geophysical and geological purposes (ADALGEO). *Computers & Geosciences 57*, 93–103.

Ustaszewski, M. & Pfiffner, O.A., 2008: Neotectonic faulting, uplift and seismicity in the central and western Swiss Alps. *Geological Society, London, Special Publications 298*, 231–249.

Valle, P., Færseth, R.B. & Fossen, H., 2002: Devonian-Triassic brittle deformation based on dyke geometry and fault kineamtics in the Sunnhordland region, SW Norway. *Norwegian Journal of Geology 82*, 3–17.

Vaz, D.A., Di Achille, G., Barata, M.T. & Alves, E.I., 2012: Tectonic lineament mapping of the Thaumasia Plateau, Mars: comparing results from photointerpretation and a semi-automatic approach. *Computers & Geosciences 48*, 162–172.

Viola, G., Andreoli, M., Ben-Avraham, Z., Stengel, I. & Reshef, M., 2005: Offshore mud volcanoes and onland faulting in southwestern Africa: neotectonic implications and constraints on the regional stress field. *Earth and Planetary Science Letters 231*, 147–160.

Viola, G., Kounov, A., Andreoli, M.A.G. & Mattila, J., 2012: Brittle tectonic evolution along the western margin of South Africa: more than 500Myr of continued reactivation. *Tectonophysics* 514-517, 93–114.

Wells, N.A. 1999: ASTRA.BAS: a program in QuickBasic 4.5 for exploring rose diagrams, circular histograms and some alternatives. *Computers & Geosciences 25*, 641–654.

Wise, D.U., Funiciello, R., Parotto, M. & Salvini, F., 1985: Topographic lineament swarms: Clues to their origin from domain analysis of Italy. *Geological Society of America Bulletin 96*, 952–967.

Wladis, D. 1999: Automatic lineament detection using digital elevation models with second derivative filters. *Photogrammetric Engineering & Remote Sensing 65*, 453–458.